K-space analysis of complex large-scale meta-structures using the Inhomogeneous Wave Correlation method

Giovanni Tufano, Fabrizio Errico, Olivier Robin, Christophe Droz, Mohamed Ichchou, Bert Pluymers, Wim Desmet, Noureddine Atalla

K-space analysis of complex large-scale meta-structures using the Inhomogeneous Wave Correlation method

G. Tufano[a,b,*], F. Errico[a,d], O. Robin[c], C. Droz[a], M. Ichchou[a], B. Pluymers[b,e], W. Desmet[b,e], N. Atalla[c]

[a] *Vibroacoustics & Complex Media Research Group, LTDS-CNRS UMR 5513, École Centrale de Lyon, Écully, 69134, France*
[b] *Noise and Vibration Research Group, PMA, KU Leuven, Celestijnenlaan 300 B, B-3001, Heverlee, Belgium*
[c] *GAUS, Université de Sherbrooke, 2500 Boulevard de l'Université, Sherbrooke, QC, J1K 2R1, Canada*
[d] *Pasta-Lab, Dipartimento di Ingegneria Industriale, Università degli Studi di Napoli Federico II, Napoli, 80125, Italy*
[e] *DMMS core lab, Flanders Make, Belgium*

Abstract

An inverse wavenumber identification tool is used to characterize the vibration behavior of three structures and meta-structures with different complexity levels: a plane steel panel, a curved thick composite sandwich shell and a stiffened aluminum aircraft sidewall panel. Bare structures are first studied and then equipped with spatially distributed small-scale resonators, leading to meta-structures. For the two curved panels, tests are conducted under diffuse acoustic field and point mechanical excitations.

For each studied case, the effect of the industrially-oriented small-scale resonators is highlighted using frequency and wavenumber analysis, showing general attenuation of the vibration level and even band gaps occurrence. The complex wavenumber identification allows also estimating the structural loss factor in the composite sandwich panel, while the multi-modal behavior is captured in the aluminum aircraft sidewall panel.

Keywords: local resonances, wavenumber, dispersion curves, vibrations control, periodic structures, meta-structures

1. Introduction

In the aerospace sector, curved shells and axial-symmetric structures are widely used. The presence of stringers and frames in the longitudinal and circumferential direction of aircraft fuselages lets assume a certain degree of structural periodicity which, if properly designed, can give some advantages in the vibroacoustic response.

Composite materials are more and more used in this sector, to fulfill the requirements of reduced structural weight and high mechanical performances. The anisotropic behavior and the complexity related to their composite nature make the development of an analytical theory or of a predictive model very hard to obtain. The vibro-acoustic response and the dynamical behavior of laminated composite sandwich shells are of fundamentals relevance for the industry. The identification of the energy propagation, of the waves

*Corresponding author
Email address: giovanni.tufano@ec-lyon.fr (G. Tufano)

attenuation, with the related damping informations, and of the waves dispersions characteristics are relevant aspects to fully describe the vibro-acoustic behavior of a system [1]. Some semi-analytical approaches have been developed in order to estimate the mechanical properties of sandwich composite structures [2, 3, 4, 5]. These formulations are limited to the low-frequency domain, in which the modes are well defined; in the mid-high-frequency range, classical analytical approaches do not give a good estimation of the waves dispersion characteristics, due to an high modal density. As alternatives, in a wave propagation framework, for the parameter identification other methods based on the wavenumber domain (k-space) analysis [6, 7, 8, 9] or based on the Statistical Energy Analysis (SEA) [10, 11, 12] are introduced.

Some applications of the Prony's method to the wavenumber analysis of two-dimensional structures have been proposed [13]. The Prony technique is a means of identifying the constituent complex wavenumbers and their corresponding amplitudes in an exponential model of the spatial response. It is a two-steps process: the wavenumbers are first found and the amplitudes for these wavenumbers are then obtained from a linear least-squares fit of the model to the data. A modified extended technique based on Prony method to estimate the complex wavenumbers is shown in Grosh et al. [14]. Ferguson et al. [15] proposed a technique to identify the dominant wavenumber in a considered area, using a windowed field of the displacement of the structure, computing the correlation between the normal velocity measurement and an harmonic wave-field. An algorithm for the identification of the complex wavenumber and of the damping loss factor was developed by Berthaut et al. [8, 9, 16]; the proposed method is called Inhomogeneous Wave Correlation (IWC) method and it allows to identify the complex flexural wavenumber in the broadband frequency range.

In order to increase the waves attenuation in certain frequency band or to generate some band gaps, periodic adds-on and locally resonant devices are widely used. The effect of wave propagation in ribs-stiffened plate structures is investigated in [16, 17], showing the multi-modal behavior in the wavenumber domain, in terms of uncoupled plate and stringer flexural wavenumbers. A vibroacoustic study of a fluid-loaded ribbed plate is shown in Maxit [18], where the response is investigated in the wavenumber domain using a discrete Fourier Transform based approach. A numerical investigation of the IWC method on curved shells and axial-symmetric structures is presented in [19], showing a good prediction of the angle-dependent wavenumber at different excitation frequencies and compared with the Fast Fourier Transform technique. For what concerns the stop bands behavior of tuned resonators, Claeys et al. [20, 21] have demonstrated their potential use to reduce the vibrational response of panels, spatially distributing them over the panel surface. An application of the IWC method on a metamaterial plate with distributed resonators is given by Van Belle et al. [22].

An experimental investigation on the vibroacoustical response of a cylindrical shell is presented in Williams et al. [23], where the dominant wavenumbers are well identified in the regions close to the natural frequencies of the structure. An analysis in the wavenumber domain is used in Photiadis et al. [24] to investigate the acoustic response of a ribbed shell, demonstrating the dominant flexural behavior in the mid-frequency range. Photiadis et al. [25] investigated the effect of distributed internal oscillators on the acoustic response of a complex ribbed shell, showing their influence in the wavenumber domain compared to the bare configuration.

The effect of the internal frames on the vibroacoustic response of an aluminum cylinder is performed by Meyer et al. [26], providing a better understanding of frames' influence in the wavenumber domain and on the dispersion curves, mainly based on the numbers and the spatial distribution of the internal frames.

Nateghi et al. [27, 28] have discussed and experimentally validated that by adding locally resonating structures to cylindrically curved panels and pipes, improved noise and vibration behavior can be obtained in a targeted and tunable frequency band. This concept was applied on an aircraft sidewall panel by Droz et al. [29] , improving the acoustic properties of the panel in the ring frequency region, showing how a smart design of metamaterial structures can be adopted to improve the vibroacoustic performance.

This work is fully devoted to the experimental identification of the dispersion characteristics of these complex structures, subjected to either a diffuse acoustic field or a point mechanical excitations. Each considered structure is first tested alone, and then with the addition of spatially-distributed small-scale resonators. The method used in this work is an extended version of the IWC method, introducing the effect of the local dynamics of the resonators and the effect of the acoustic excitation, in presence of periodic adds-on. The main advantages of this method are the possibility to investigate both in-plane and curved structures, the identification of the resonators related band gaps and the use of the experimental measured data, without any restriction related to an ordered mesh-grid for the acquisition points.

In section 2, an overview of the IWC method is presented and an extended formulation to take in account the curvature effect is developed. The experimental set-up for each studied case is fully described in section 3, showing how the experimental tests were performed and giving information about the tuning frequencies of the resonators. The section 4 is fully devoted to the results discussion; the isotropic steel panel is first considered, then all the results concerning the curved structures are discussed. A numerical simulation on an isotropic curved panel is performed to validate the feasibility of the proposed IWC formulation for curved structures, followed by experimental results on the two considered curved structures for tests.

2. Overview of the Inhomogeneous wave correlation method and new formulation for curvature effect

The method developed in this work is derived from the *Inhomogeneous Wave Correlation* (IWC) method. The inverse approach here proposed is extended to complex curved structures in presence of periodic elements and small-scale resonators. The aim of this approach is the complete description of the angle-dependent dispersion characteristics and the identification of the structural damping information of a vibrating structure, using the whole wave field of a vibrating structure as primary input [8, 9, 16, 30, 31]. This method calculates the correlation between the energy carried on by an inhomogeneous traveling wave and the total energy of the vibrational field. Considering a plane structure and a plane wave approach, the inhomogeneous wave can be expressed as follows:

$$\tilde{w}_{k_{\mathbb{C}},\theta}(x,y) = \exp\{-ik_{\mathbb{C}}(\theta)(x\cos\theta + y\sin\theta)\} \tag{1}$$

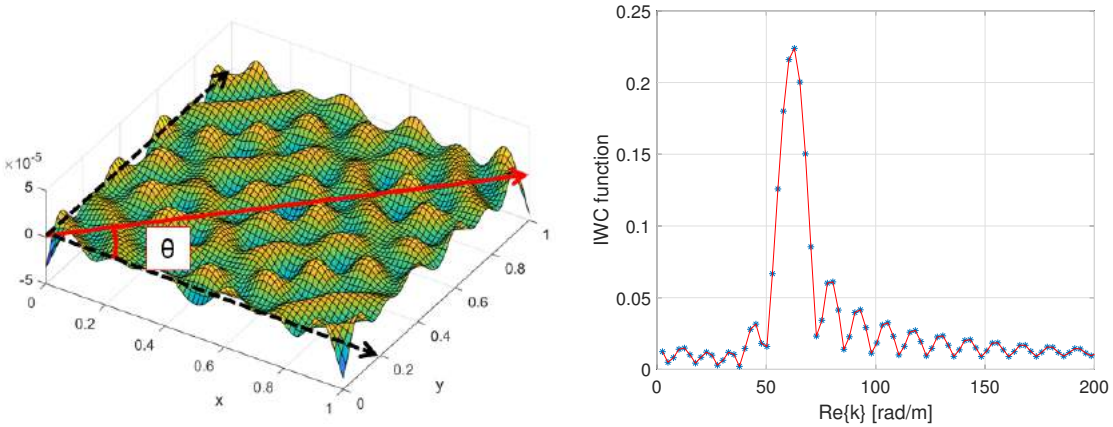

(a) (b)

Figure 1: Schematic representation of the IWC algorithm: vibrational field and propagative plane wave (a) and IWC correlation function (b)

where θ is the angle of propagation and $k_{\mathbb{C}} = k_{\Re} + ik_{\Im}$ is the complex wavenumber, which contains both propagation and attenuation informations. At each frequency f and for a given direction θ, the unknown complex wavenumber $k_{\mathbb{C}}$ can be identified as the location of the maximum of the normalized correlation function, denoting the point where the measured signal $\hat{w}$ correlates best with the inhomogeneous wave $\tilde{w}_{k_{\mathbb{C}},\theta}(x, y)$:

$$\mathcal{I}(k_{\mathbb{C}}, \theta) = \frac{\left| \iint_{\Omega} \hat{w} \cdot \tilde{w}^*_{k_{\mathbb{C}},\theta} \, dx \, dy \right|}{\sqrt{\iint_{\Omega} |\hat{w}|^2 \, dx \, dy \cdot \iint_{\Omega} |\tilde{w}_{k_{\mathbb{C}},\theta}|^2 \, dx \, dy}} \tag{2}$$

where * denotes the complex conjugate. Rewriting Eq. 2 in the discrete domain, the integration over the entire surface Ω is replaced by a finite weighted sum:

$$\iint_{\Omega} dx \, dy \Longrightarrow \sum_{j=1}^{N} h_j \Omega_j \tag{3}$$

where h_j is the coherence of the measured signal at each point ($h_j = 1$ if the coherence is not available), Ω_j is an estimation of the surface around the point j and N is the total number of acquisition points. Introducing Eq. (3) into Eq. (2), the correlation function becomes

$$\mathcal{I}(k_{\mathbb{C}}, \theta) = \frac{\left| \sum_{j=1}^{N} \hat{w}(x_j, y_j) \cdot \tilde{w}^*_{k_{\mathbb{C}},\theta}(x_j, y_j) h_j \Omega_j \right|}{\sqrt{\sum_{j=1}^{N} |\hat{w}(x_j, y_j)|^2 h_j \Omega_j \cdot \sum_{j=1}^{N} |\tilde{w}_{k_{\mathbb{C}},\theta}(x_j, y_j)|^2 h_j \Omega_j}} \tag{4}$$

The algorithm first puts angle θ into a discrete set of values; for each of these angles, the maximum of IWC is located at a value $(k_{\Re}, k_{\Im})$, creating two functions $\theta \to k_{\Re}(\theta)$ and $\theta \to k_{\Im}(\theta)$ defined on a set of discrete values of θ. A schematic representation of the IWC algorithm is shown in Fig. 1.

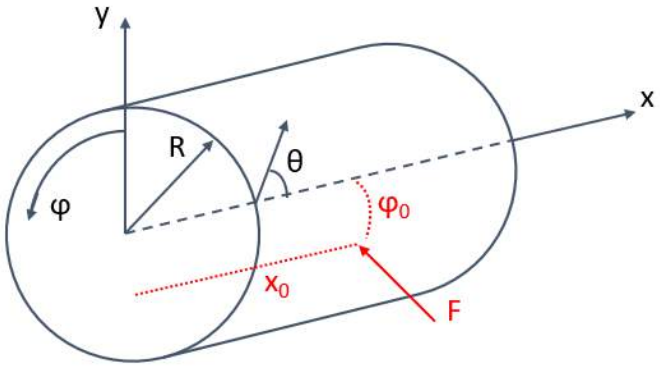

Figure 2: Curved structure coordinates system

From the identified structural wavenumber, k, the k_x and k_y components in the x and y direction are defined by

$$\begin{aligned} k_x &= k\cos\theta \\ k_y &= k\sin\theta \end{aligned} \tag{5}$$

The full complex dispersion relation is calculated by a repetition of the algorithm on the whole frequency band of interest.

For point harmonic excitations, the estimate of the decaying part of the wavenumber can be improved by taking in account the location of the excitation (x_0, y_0) [22]. The spatially decaying plane wave assumes the following expression:

$$\tilde{w}_{k_\mathbb{C},\theta}(x,y) = \exp\{-ik_\mathbb{C}(\theta)((x-x_0)\cos\theta + (y-y_0)\sin\theta)\} \tag{6}$$

Based on this initial description, a new formulation for curved structures can be derived, which takes in account the curvature effect in the IWC formulation. From the notations and the coordinates system shown in Fig. 2, identifying with R the curvature radius of the structure and with φ the angular coordinate, the following relationships can be derived:

$$y = R\sin\varphi \approx R\varphi \quad \text{and} \quad k_\varphi = Rk_y \tag{7}$$

where a small value of the angle φ is assumed (this value strictly depends on the discretization resolution). Substituting these relationships in the expression of the inhomogeneous wave, we obtain:

$$\tilde{w}_{k_\mathbb{C},\theta}(x,\varphi) = \exp\{-ik_\mathbb{C}(\theta)((x-x_0)\cos\theta + (\varphi-\varphi_0)\sin\theta)\} \tag{8}$$

where φ_0 is the angular position of the excitation point.

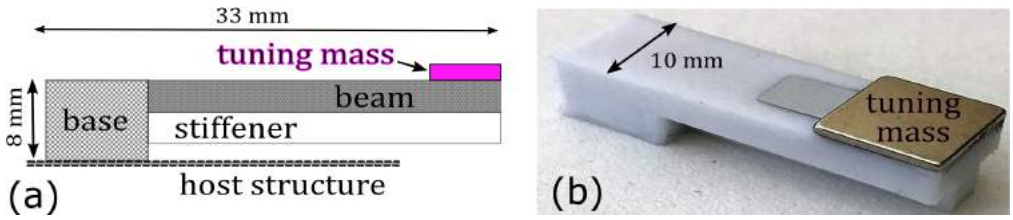

Figure 3: Schematic representation of the resonator (a) and its application on the host structure (b)

Moving from the Cartesian coordinate system to the curved one, Eq. 4 is modified as follows

$$\mathcal{I}(k_{\mathbb{C}},\theta) = \frac{\left|\sum_{j=1}^{N} \hat{w}(x_j,\varphi_j)\cdot \tilde{w}^{*}_{k_{\mathbb{C}},\theta}(x_j,\varphi_j) h_j \Omega_j\right|}{\sqrt{\sum_{j=1}^{N}|\hat{w}(x_j,\varphi_j)|^2 h_j\Omega_j \cdot \sum_{j=1}^{N}|\tilde{w}_{k_{\mathbb{C}},\theta}(x_j,\varphi_j)|^2 h_j\Omega_j}} \tag{9}$$

The location of the maximum of the correlation function $\mathcal{I}(k_{\mathbb{C}},\theta)$ gives the identified complex wavenumber in the specified direction. When the structure is complex, the correlation function could be characterized by an absolute maximum and some other local maxima, denoting the presence of different bending waves propagating at the same time. Following the evolution of the local maxima, the multi-modal behavior of the structure can be described, as shown in section 4.3.

3. Experimental methods

Three different structures have been experimentally investigated: an isotropic steel plane panel, a thick curved composite laminated sandwich panel and a thin aluminum aircraft sidewall panel, including frames and stringers. The resonator is schematically represented in Fig. 3; the shape is similar to a cantilever beam, with a rectangular prism base of dimensions 10 x 10 x 8 mm^3 and a magnet glued on the opposite side, with the possibility to tune it by adding or removing the magnet masses. The resonators are 3D-printed using polycarbonate polymer, with a total dimensions of 33 x 10 x 8 mm^3 and a unit weight of 2.72 g. The resonator main beam has dimensions 23 x 10 x 4 mm^3 and the stiffener element has section of 4 x 3.5 mm. The concept of the resonators and their feasibility in reducing the bending wavenumber was demonstrated in [32]. The same concept was used in [29], in which they were also tested on the aluminum aircraft sidewall panel considered in the present work, with the aim to improve the sound insulation properties of the considered structure. A schematic representation of the resonator and its application on the host structure are shown in Fig. 3. A uniform distribution of the resonators on the surface of the structures is chosen to avoid any local and/or directional effect.

3.1. Isotropic plate

An isotropic steel plate of dimensions 0.95 m x 0.6 m and thickness of 2 mm is considered. The host structure has a total weight of 9 kg, approximatively. To simulate free boundary conditions, the structure was suspended at three points along the longer edge using Polylactic Acid filaments. The plate was excited by a point mechanical force using a Brüel & Kjær shaker attached to the host structure using an impedance

Figure 4: Set-up of the steel plate with distributed resonators

head (Fig. 4). The out of plane vibrational field was acquired using a Polytec PSV-500 Scanning Vibrometer. An acquisition window of 0.92 m x 0.56 m was scanned, using a mesh of 60 x 24 along length and width, respectively, with a total number of 1440 acquisition points. The bare structure was first tested, and then the effect of distributed resonators tuned at frequencies of 800 Hz and 1400 Hz were successively tested. The resonators frequency being adjusted with varying tuning masses, the added weight was different for the two considered frequencies. For the first one (800 Hz), the added weight from the resonators represented 2.5% of the total panel weight, while for the second one (1400 Hz), the panel weight was increased by 1.5%.

The shaker and the resonators were mounted on the rear surface of the host structure while the front one was scanned by the Laser Doppler Velocimeter system. The excitation was generated using a white noise signal from 100 Hz to 2000 Hz. A schematic representation of the distributed resonators and of the experimental set-up is shown in Fig. 4.

3.2. Curved composite sandwich panel

The composite panel dimensions are 1.54 m x 1.62 m, with a curvature radius approximatively of 0.97 m, and thickness equal to 27.5 mm (Fig. 5a).

A preliminary experimental investigation of the dispersion characteristics of the composite laminated sandwich panel was first conducted. The panel has been simply hanged in the anechoic room assuming free boundary conditions. The tests are performed using an impact hammer and four accelerometers, placed in the circumferential and axial directions; the experimental data have been recorded using a Brüel & Kjær real-time, multichannel sound and vibration data acquisition card. The experimental wavenumbers were calculated using the phase difference between the accelerometers, placed along the specific direction [33, 34]. The recorded time data were filtered in the time domain to eliminate the reverberant field contribution.

The panel was then installed in the aperture between the coupled reverberant-anechoic rooms of the GAUS (*Groupe d'Acoustique de l'Université de Sherbrooke*) laboratory, at Université de Sherbrooke (Fig. 5). The representative scheme of the coupled rooms is shown in Fig. 6. The reverberant room has dimensions

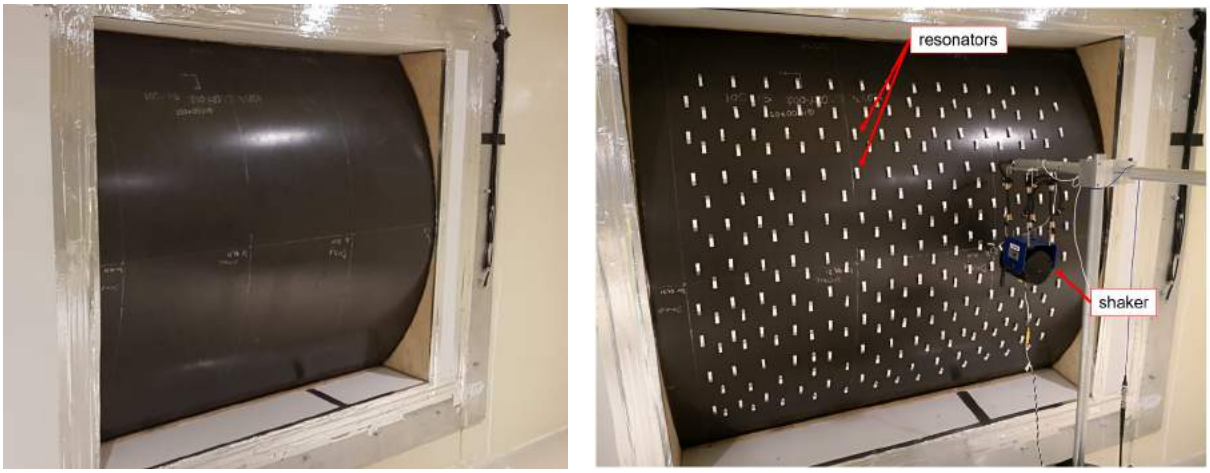

(a) (b)

Figure 5: Curved composite laminate sandwich panel: bare configuration (a) and distributed resonators configuration (b)

7.5 x 6.2 x 3.0 m^3 with an averaged reverberation time (T_{60}) of 5.5 s in the frequency band [50 Hz - 1000 Hz]. The acoustic excitation was generated by a loudspeaker placed close to a corner of the room, with a white noise signal input from 100 Hz to 3000 Hz. Concerning the mechanical excitation, a Modal Shop Model 2025E shaker was installed in the reverberant room and attached to the test structure using an impedance head, as shown in Fig.5b; the excitation was generated using a white noise signal from 100 Hz to 3000 Hz. The full vibrational field was measured using a Polytec 3D Scanning Vibrometer (PSV-3D), installed in the anechoic room, with dimensions 6.0 x 7.0 x 3.0 m^3. The acquisition window was approximatively of 1.2 m x 1.0 m, in order to be sufficiently far from the boundaries and to reduce the influence of the boundary conditions, with a total number of 3111 measured points (mesh grid of 61 x 51).

A distributed pattern of 3D-printed small-scale resonators was then attached to the panel and compared to the bare test case (Fig. 5b). The chosen tuning frequency was 1000 Hz; the panel weight was increased by 4% for a total number of 246 resonators. For each considered excitation (diffuse acoustic field (DAF) and point mechanical excitation), the bare structure was first tested, and then the effect of distributed resonators tuned at a frequency of 1000 Hz was tested. In the reverberant room, a control microphone was placed close to the surface of the excited structure to double check the incident pressure and normalize the FRFs (Frequency Response Functions).

3.3. Aluminum aircraft sidewall panel

The aluminum panel has dimensions 1.45 m x 1.70 m, with a curvature radius approximatively of 1.30 m and a thickness of 1.2 mm (Fig. 7). The panel was installed in the aperture between the coupled reverberant-anechoic rooms of the GAUS laboratory, already described in the section 3.2. For the point mechanical excitation, the bare panel was first tested with free boundary conditions. For the diffuse acoustic field excitation, the bare structure was first tested and the effect of distributed resonators tuned at three different

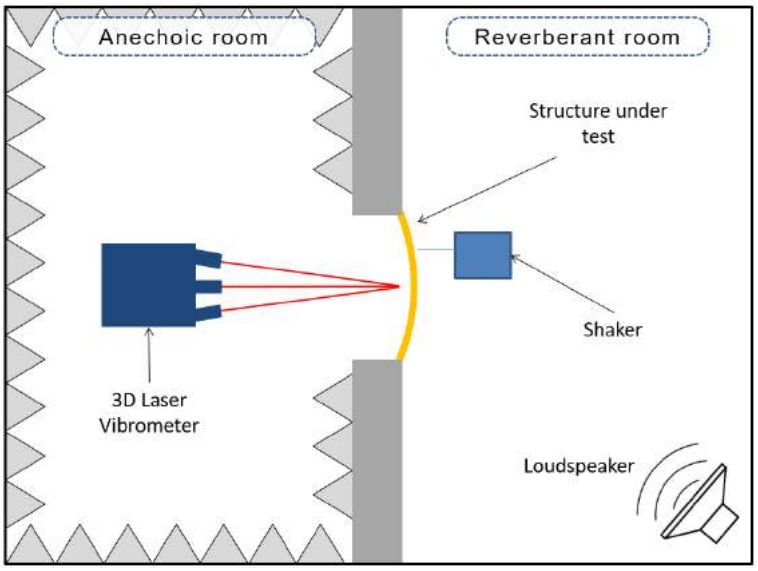

Figure 6: Illustration of the coupled rooms

frequencies was then tested. The resonators were tuned at three different frequencies, equally distributed; the chosen frequencies were 670 Hz, 820 Hz and 980 Hz, in order to cover a relatively large frequency band. The presence of the 246 resonators increased the panels weight by 4.5% in this case.

The same Modal Shop Model 2025E shaker, described in the section 3.2, was used to excite the aluminum panel, using a white noise signal input from 100 Hz to 2000 Hz. The structure was freely suspended to simulate free boundary condition; the shaker was placed on an internal frame structure, as shown in Fig. 8a. The external surface was scanned using a Polytec 3D Scanning Vibrometer, with an acquisition window of approximatively of 0.85 m x 0.95 m, with 5451 acquisition points (equivalent to a mesh grid of 69 x 79). To test the aluminum panel under diffuse acoustic field excitation, the panel was installed between the two rooms, as shown in Fig. 7. The resonators were attached on the external surface (in the reverberant room) and the internal surface was scanned by a Polytec 3D Scanning Vibrometer, in the skin regions between stringers and frames, as shown in Fig. 9a; the total number of scanned points was 2916, with a mesh grid of 27 x 9 for each region (total mesh grid of 54 x 54).

4. Numerical validations and experimental results

Firstly, the proposed IWC formulation for curved structures is numerically validated. The method is applied on an isotropic curved panel; the employed material is a standard aeronautical aluminum alloy, similarly to the experimental measured case. The dimensions are 0.85 m x 0.95 m, thickness equal to 1.2 mm and curvature radius of 1.3 m. The finite element model of this structure, shown in Fig. 10a , is built using 13328 shell structural elements (ANSYS SHELL181), with a total number of degrees of freedom equal to 81560. A point mechanical force is positioned as it was made for experiments. The analysis is performed in the frequency range from 100 Hz to 2000 Hz. The dispersion curve obtained with the proposed approach

(a) (b)

Figure 7: Set-up and installation of the bare configuration: outer skin subjected to DAF excitation (a) and inner surface (b)

(a) (b)

Figure 8: Set-up and installation for mechanical excitation: shaker installation (a) and acquisition region (b)

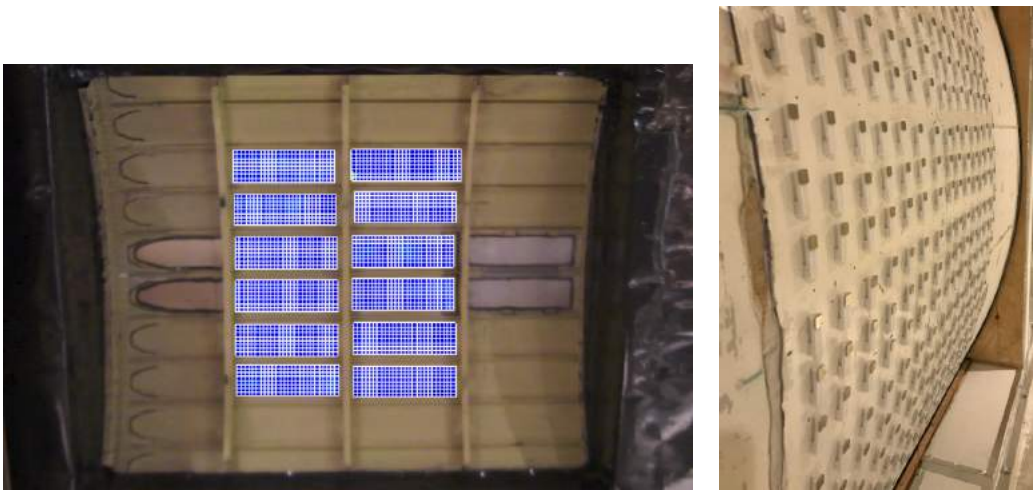

(a) (b)

Figure 9: DAF excitation: acquisition window (a) and detail of the host structure and the resonators (b)

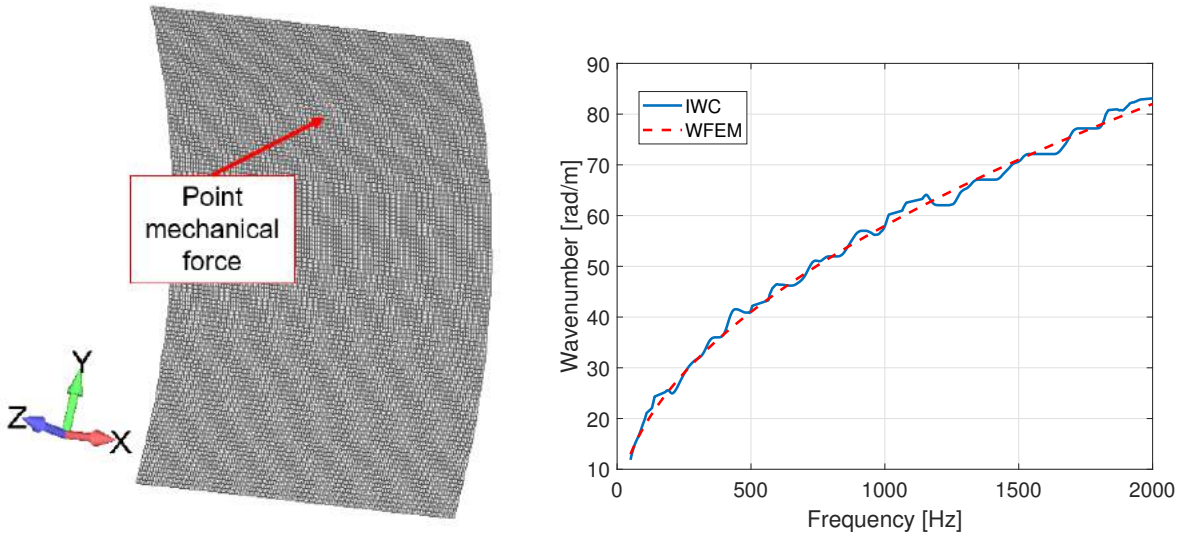

(a) (b)

Figure 10: FE model of the curved panel (a) and dispersion curves comparison (b)

is validated by the Wave Finite Element Method (WFEM) [35, 36, 37, 38] ; the dispersion curves are in agreement on the whole frequency range, as shown in Fig. 10b.

4.1. Steel plate: experimental results and validation

In this case, the dispersion curves obtained with the IWC method is compared with the classical Kirchhoff's thin plate theory. An analytical expression of the dispersion relation can be derived from this theory, obtaining the following expression for the flexural wavenumber

$$k = \sqrt{\omega}\left(\frac{\rho h}{D}\right)^{1/4} \tag{10}$$

where ρ is the mass density, h is the plate thickness and D is the bending stiffness.

The dispersion curves are estimated for all tested configurations and compared with the analytical solution, as shown in Fig. 11. The estimated dispersion curves are in agreement with the analytical solution in the whole frequency range. In Fig. 11a, the effect of the resonators tuned at 800 Hz is shown, giving a band gap of approximatively 200 Hz width; before and after the band gap, the dispersion curve follows the one of the bare configuration and the analytical solution. For what concerns the resonators tuned at 1400 Hz, the originated band gap width is of approximatively 250 Hz, as shown in Fig. 11b. For both configuration, a strong attenuation is observed in the resonators tuning frequency regions.

4.2. Curved composite laminated sandwich panel: experimental results and validation

Firstly, the Frequency Response Functions (FRFs) of the two configurations of the panel are compared, for both excitations (Fig. 12). For what concerns the FRF of the panel under diffuse acoustic field excitation, the natural modes are not well identified due to the high damping level; in any case, around the tuning frequency

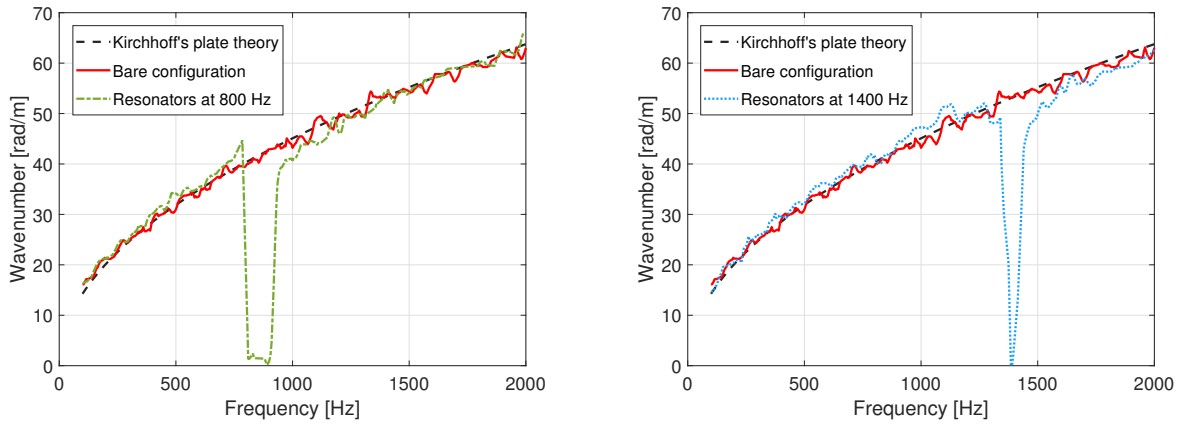

(a) (b)

Figure 11: Dispersion curves comparison for the steel plate, with and without the resonators: at 800 Hz (a) and at 1400 Hz (b)

of the resonators a drop of amplitude is observed (Fig. 12a). Under mechanical excitation, the natural modes of the structure can be easily identified; the drop around the tuning frequency of the resonators is clearer, as shown in Fig. 12b.

The measured displacement fields for all four configurations and for both excitation condition are plotted in Fig. 13, choosing a frequency around the tuning frequency of the resonators. To make a comparison between the experimental displacement fields, all the displacements have been normalized by the maximum value. Fig. 14 shows the bending dispersion curves under diffuse acoustic field excitation for both configurations, with and without resonators; the dispersion curves are computed in the two orthogonal directions, axial and circumferential. For both directions, the local dynamics of the resonators is well described.

The same comparison is done using the mechanical excitation, as shown in Fig. 15; the dispersion curves are calculated in both directions, with and without the resonators. The local dynamics of the resonators is well described in both directions.

From the estimation of the complex wavenumbers, a calculation of the damping loss factor is performed, using the following relationship between the real and imaginary part of the wavenumber

$$\eta = \left| \frac{k_{\Im}^4}{k_{\Re}^4} \right| \tag{11}$$

The experimental damping loss factor is calculated for both configuration, the test case and the panel with distributed resonators, as shown in Fig. 16a, where the damping loss factor is expressed in one twelfth octave band. In low frequency region, the damping loss factor appears very high, mainly due to the boundary conditions influence. Around the tuning frequency of the resonators an increase of the damping factor is present; this effect is correlated to the continuously increasing of the imaginary part of the wavenumber and decreasing of the real one, consequently to a strong reduction of the vibration level.

A different method derived from the Statistical Energy Analysis (SEA) is used to estimate the damping loss

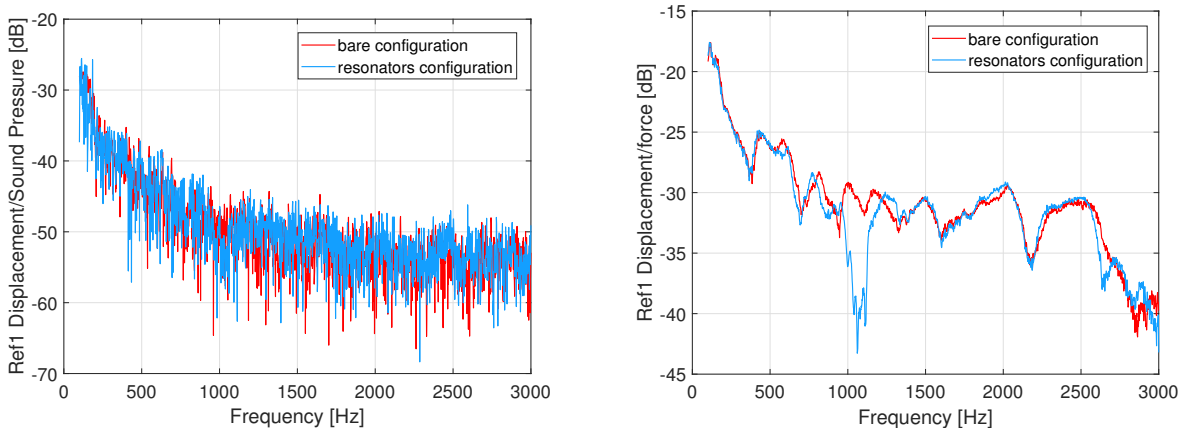

(a) (b)

Figure 12: FRFs comparison for both configurations and excitations: DAF excitation (a) and point mechanical excitation (b)

factor: the power input method (PIM). The basic idea is that, in steady-state condition, the input power is equal to the dissipated power [1]. The damping loss factor is expressed by

$$\eta_f = \frac{P_f}{\omega E_f} \tag{12}$$

where P_f is the input power and the E_f is the total energy, averaged in the frequency band. Input power and total energy are calculated by the following expressions, respectively

$$P_f = 0.5 \cdot \Re(F * v) = 0.5 \cdot \Re\left(\int_{\omega_1}^{\omega_2} G_{Fv}(\omega)\, d\omega \right) \tag{13}$$

$$E_f = M_f v_f^2 = M_f \left(\int_{\omega_1}^{\omega_2} G_{vv}(\omega)\, d\omega \right) \tag{14}$$

where G_{Fv} is the cross-spectral density between the force F and the velocity v, M_f is the mass related to the measurement area and G_{vv} is the auto-spectral density of the velocity. The quadratic velocities and the force are averaged over 200 points. All these quantities are derived from the use of an impedance head.

4.3. Aluminum aircraft sidewall panel: experimental results and validation

The finite element model of the panel is built and shown in Fig. 17; the numerical displacement field is obtained by a full FE analysis, using a point harmonic excitation at the same location of the shaker in the experimental test. The material properties introduced in the numerical model are of a standard aluminum alloy for aeronautical application: Young's modulus $E = 73.1\,\mathrm{GPa}$, mass density $\rho = 2780.0\,\mathrm{kg\,m^{-3}}$ and Poisson coefficient $\nu = 0.33$. The structure is not modeled with a very high degree of fidelity. For example, the all the joints and connections are not modeled, stringers and frame are considered rigidly connected; the small air-gap present in the real structure is neglected and some small holes in the frames structure are not

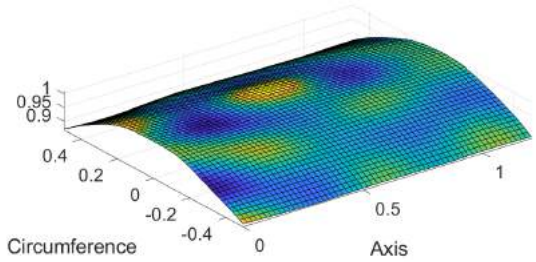

(a)

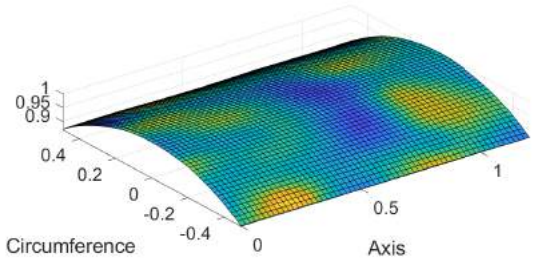

(b)

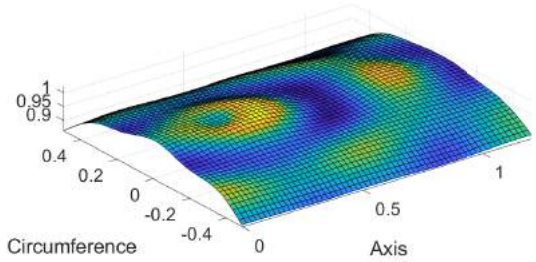

(c)

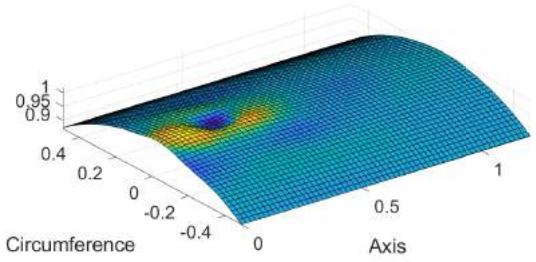

(d)

Figure 13: Normalized displacement fields, with and without the effect of the resonators: bare test case under DAF excitation (a), resonators configuration under DAF excitation (b), bare test case under shaker excitation (c) and resonators configuration under shaker excitation (d)

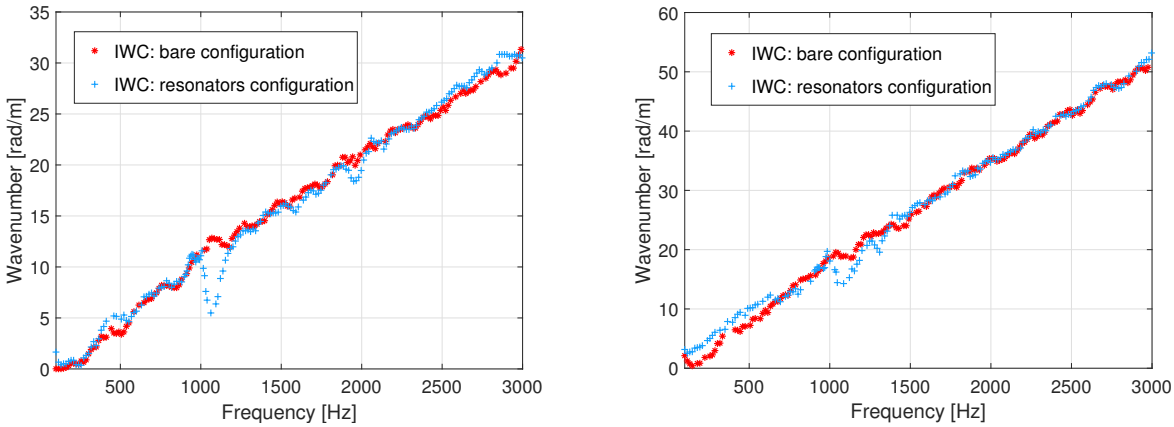

(a) (b)

Figure 14: Dispersion curves under DAF excitation, with and without resonators: axial (a) and circumferential (b) directions

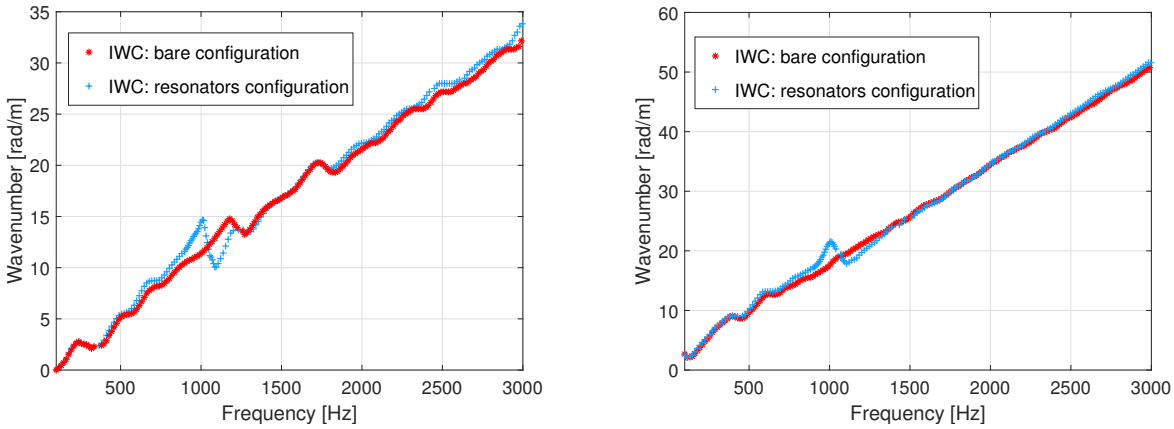

(a) (b)

Figure 15: Dispersion curves under shaker, with and without resonators: axial (a) and circumferential (b) directions

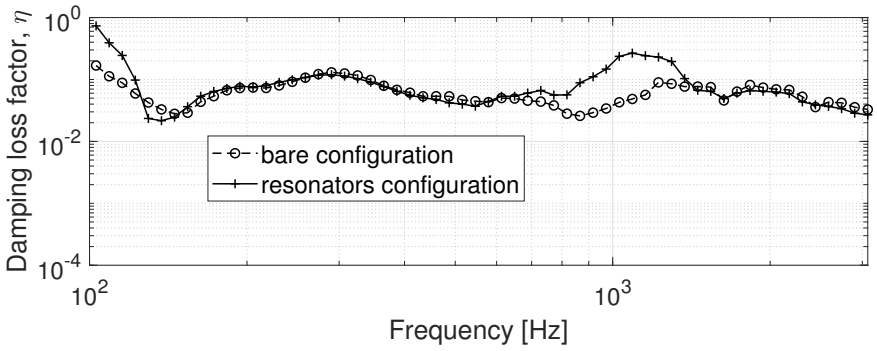

(a)

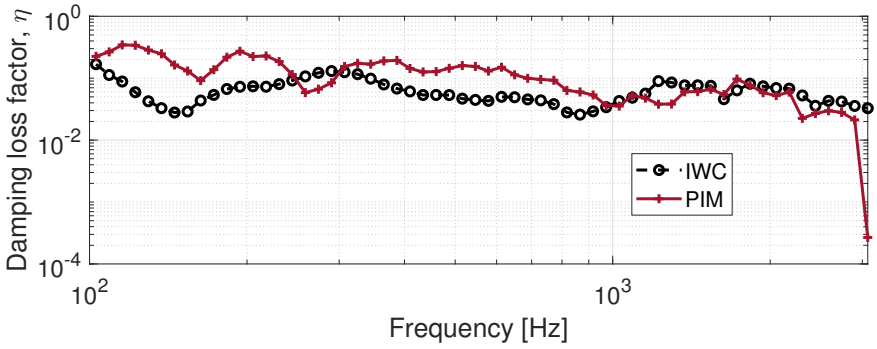

(b)

Figure 16: Damping Loss Factor estimation: bare test case and resonators configuration comparison with Eq. 11 (a) and bare test case comparison between Eq. 11 and PIM (b)

present in the numerical model, because their effect on the dispersion characteristics is considered of small influence. The FE model is built using shell elements (ANSYS SHELL181); the total number of structural elements is approximatively of $3.2 \cdot 10^4$. The normal displacements of the nodes of the external surface are used as primary input in Eq. 9; from the full-field measurement, the multi-modal behavior is well identified in the numerical simulation and experimental test, with shaker excitation and full-field acquisition, as shown in Fig. 18a. The two different modes of propagation are quite evident in the axial direction and they are well captured when the full-structure is scanned. The same behavior is not captured when the acquisition window is reduced to the internal bays (as shown in Fig. 9a), because the stringers vibration is not acquired. Two uncoupled wavenumber are identified at the same frequency: plate flexural and stringer flexural. Some discrepancy between the numerical and experimental dispersion curves are present in Fig. 18a, mainly due to the modeling choices. A good agreement between the numerical dispersion curve and the experimental ones, under the two different loading conditions, is shown in Fig. 18, both in the axial and circumferential directions.

The effect of the resonators on the dispersion curves is remarkable, in both directions. In the axial direction (19a) the bending dispersion curve appears higher in frequency; in the circumferential one a band-gap between 500 Hz and 1000 Hz appears, as shown in Fig. 19b. In this frequency band, the energy flowing in structure is dissipated by the vibration of the resonators, showing an high apparent stiffening behavior (lower values of the wavenumbers compared to the bare test case).

5. Conclusions

In this paper, the feasibility of the Inhomogeneous Wave Correlation method on complex structures, in presence of a local dynamics effect and under diffuse acoustic field excitation have been demonstrated, giving a good estimation of the dispersion curves for all tested configurations. The global bending behavior of the aeronautical aluminum panel is well captured, even if the acquisition window is reduced to the bays between the stringers and the frames. At the same time, the local dynamics and the multi-modal behavior is not described. This is one of the main advantages of the proposed approach, which allows to describe the global behavior from a reduced acquisition window and a reduced number of points. The efficiency of this 3D-printed small-scale resonators is also demonstrated, obtaining a reduction of the vibrational field of the panels. For all tested configuration, in the frequency band the resonators are tuned to work in, a drop in the dispersion curves is observed. The method described in this work is mainly an energetic approach, which makes a correlation between the energy carried on by the inhomogeneous wave and the total energy of the vibrating structure. The drops in the dispersion curves appear because the energy flow in the structure is strongly reduced and dissipated by the resonators.

This preliminary study on the industrial application of small-scale resonators on real aeronautic structures opens the possibility to attenuate the vibration level in some specific frequency bands, working on the design

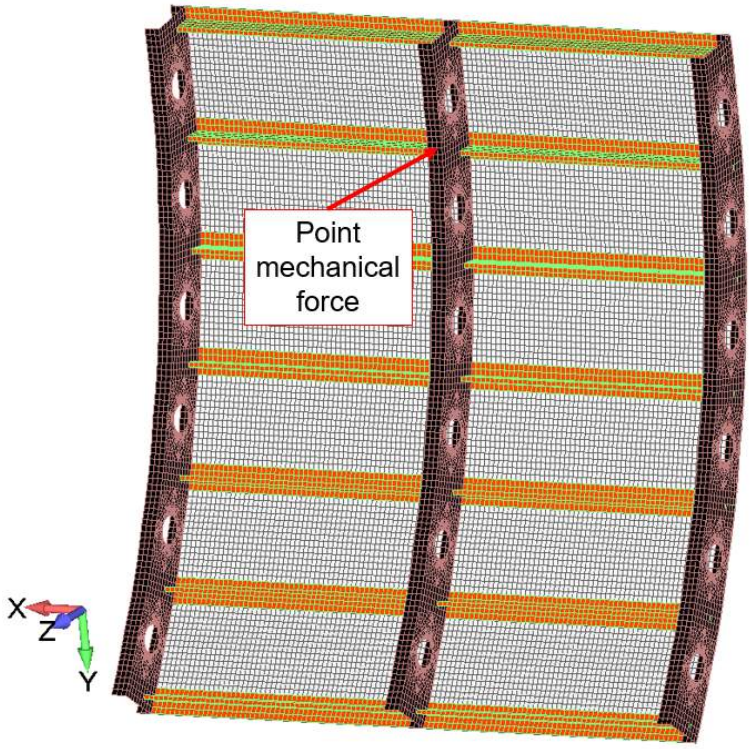

Figure 17: Finite element model of the aluminum panel

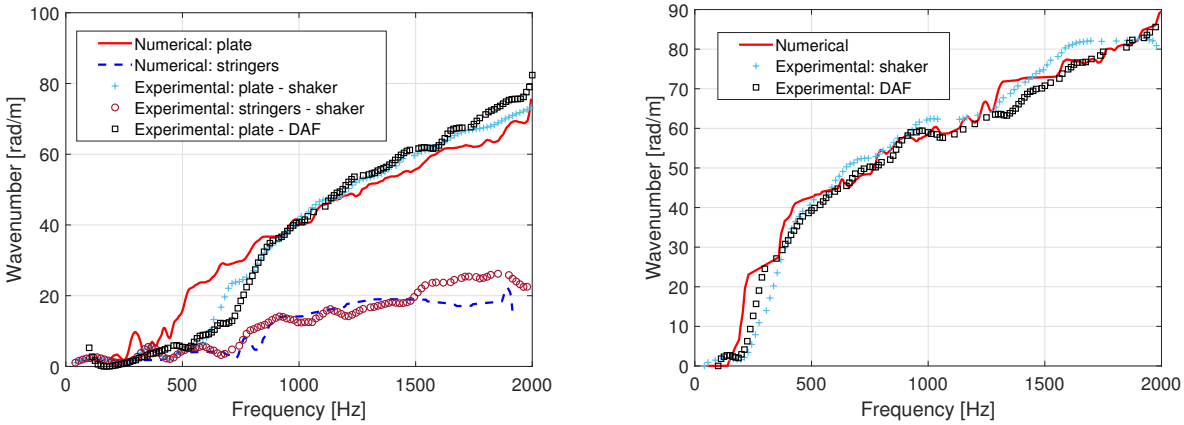

(a) (b)

Figure 18: Dispersion curves for the bare configuration and different loading conditions: axial (a) and circumferential (b) directions

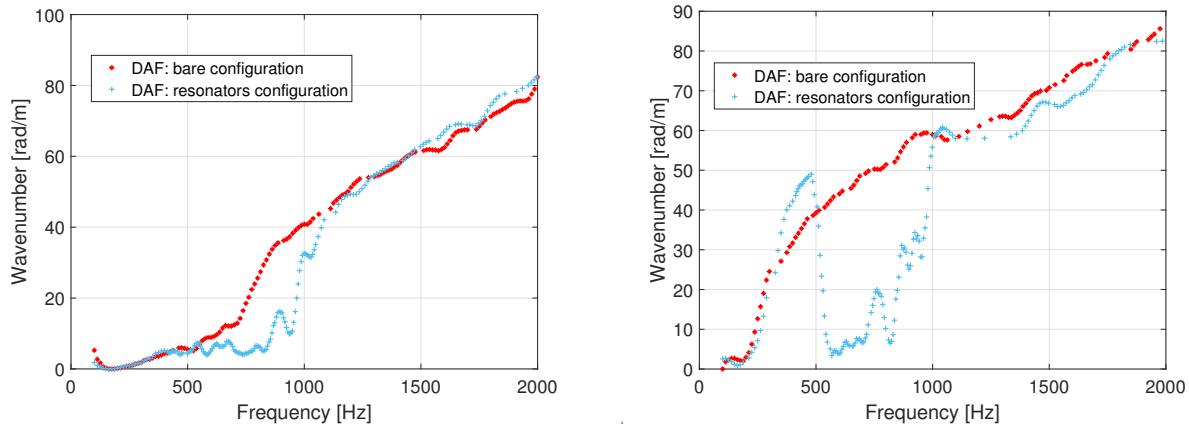

Figure 19: Dispersion curves under DAF excitation, with and without resonators: axial (a) and circumferential (b) directions

of the resonators. A deep investigation about the design of the resonators can be done in order to increase the waves' attenuation and to enlarge the band-gap and the resonance zone.

Acknowledgment

This project has received funding from the European Union's Horizon 2020 research and innovation program under the Marie Sklodowska-Curie grant agreement No. 675441. The authors would like to acknowledge Maxime Bilodeau for his help in the installation and set-up of the 3D laser vibrometer. Patrick Levesque is also acknowledged for the installation of the panels in the reverberant room.

References

[1] R. Cherif, J.-D. Chazot, N. Atalla, Damping loss factor estimation of two-dimensional orthotropic structures from a displacement field measurement, Journal of Sound and Vibration 356 (2015) 61–71. doi:10.1016/j.jsv.2015.06.042.

[2] E. Nilsson, A. C. Nilsson, Prediction and measurement of some dynamic properties of sandwich structures with honeycomb and foam cores, Journal of Sound and Vibration 251 (2002) 409–430. doi:10.1006/jsvi.2001.4007.

[3] D. Chronopoulos, B. Troclet, O. Bareille, M. Ichchou, Modeling the response of composite panels by a dynamic stiffness approach, Composite Structures 96 (2013) 111–120. doi:10.1016/j.compstruct.2012.08.047.

[4] D. Chronopoulos, M. Ichchou, B. Troclet, O. Bareille, Efficient prediction of the response of layered shells by a dynamic stiffness approach, Composite Structures 97 (2013) 401–404. doi:10.1016/j.compstruct.2012.10.012.

[5] C. Droz, O. Bareille, M. Ichchou, A new procedure for the determination of structural characteristics of sandwich plates in medium frequencies, Composites Part B 112 (2017) 103–111. doi:10.1016/j.compositesb.2016.12.023.

[6] J. G. McDaniel, W. S. Shepard-Jr., Estimation of structural wave numbers from spatially sparse response measurements, The Journal of the Acoustical Society of America 108 (2000) 1674. doi:10.1121/1.1310668.

[7] J. McDaniel, P. Dupont, L. Savino, A wave approach to estimating frequency-dependent damping under transient loading, Journal of Sound and Vibration 231 (2000) 433–449. doi:10.1006/jsvi.1999.2723.

[8] J. Berthaut, M. N. Ichchou, L. Jezequel, K-space identification of apparent structural behavior, Journal of Sound and Vibration 280 (2005) 1125–1131. doi:10.1016/j.jsv.2004.02.044.

[9] M. N. Ichchou, J. Berthaut, M. Collet, Multi-mode wave propagation in ribbed plates: Part I, wavenumber-space characteristics, International Journal of Solids and Structures 45 (2008) 1179–1195. doi:10.1016/j.ijsolstr.2007.09.032.

[10] R. H. Lyon, R. G. DeJong, Theory and Application of Statistical Energy Analysis, Butterworth Heinemann, 1995.

[11] S. Langley, Some perspective on wave-mode duality in SEA, Proceeding of the IUTAM symposium on statistical energy analysis; 1997 (1997) 1–12doi:10.1007/978-94-015-9173-7_1.

[12] D. Chronopoulos, M. Ichchou, B. Troclet, O. Bareille, Predicting the broadband response of a layered cone-cylinder-cone shell, Composite Structures 107 (2014) 149–159. doi:10.1016/j.compstruct.2013.07.055.

[13] J. S. R. Marple, Digital Spectral Analysis with Applications, Prentice-Hall, Englewood Cliffs, NJ, 1987.

[14] K. Grosh, E. J. Williams, Complex wave-number decomposition of structural vibrations, The Journal of the Acoustical Society of America 93 (1993) 836–848. doi:10.1121/1.405445.

[15] N. S. Ferguson, C. R. Halkyard, B. G. Mace, K. H. Heron, The estimation of wavenumbers in two dimensional structures, Proceeding of ISMA 2002 2 (2002) 799–806.

[16] M. N. Ichchou, J. Berthaut, M. Collet, Multi-mode wave propagation in ribbed plates. Part II: predictions and comparisons, International Journal of Solids and Structures 45 (2008) 1196–1216. doi:10.1016/j.ijsolstr.2007.08.020.

[17] U. Orrenius, S. Finnveden, Calculation of wave propagation in rib-stiffened plate structures, Journal of Sound and Vibration 198 (1996) 203–224. doi:10.1006/jsvi.1996.0565.

[18] L. Maxit, Wavenumber space and physical space responses of a periodically ribbed plate to a point drive: A discrete approach, Applied Acoustics 70 (2009) 563–578. doi:10.1016/j.apacoust.2008.06.012.

[19] G. Tufano, C. Droz, O. Bareille, A.-M. Zine, B. Pluymers, W. Desmet, M. Ichchou, Wavenumber identification technique for axial-symmetric structures, Proceeding of ISMA 2018 (2018) 4499–4508.

[20] C. Claeys, K. Vergote, P. Sas, W. Desmet, On the potential of tuned resonators to obtain low-frequency vibrational stop bands in periodic panels, Journal of Sound and Vibration 332 (2013) 1418–1436. doi:10.1016/j.jsv.2012.09.047.

[21] C. Claeys, P. Sas, W. Desmet, On the acoustic radiation efficiency of local resonance based stop band materials, Journal of Sound and Vibration 333 (2014) 3203–3213. doi:10.1016/j.jsv.2014.03.019.

[22] L. Van Belle, C. Claeys, E. Deckers, W. Desmet, On the impact of damping on the dispersion curves of a locally resonant metamaterial: Modeling and experimental validation, Journal of Sound and Vibration 409 (2017) 1–23. doi:10.1016/j.jsv.2017.07.045.

[23] E. G. Williams, B. H. Houston, J. A. Bucaro, Experimental investigation of the wave propagation on a pointdriven, submerged capped cylinder using kspace analysis, The Journal of the Acoustical Society of America 87 (1990) 513–522. doi:10.1121/1.398922.

[24] D. M. Photiadis, B. H. Houston, E. G. Williams, Wave-number space response of a near periodically ribbed shell, The Journal of the Acoustical Society of America 101 (1997) 877–886. doi:10.1121/1.418108.

[25] D. M. Photiadis, J. A. Bucaro, B. H. Houston, The effect of internal oscillators on the acoustic response of a submerged shell, The Journal of the Acoustical Society of America 101 (1997) 895–899. doi:10.1121/1.418048.

[26] V. Meyer, L. Maxit, Y. Renou, C. Audoly, Experimental investigation of the influence of internal frames on the vibroacoustic behavior of a stiffened cylindrical shell using wavenumber analysis, Mechanical Systems and Signal Processing 93 (2017) 104–117. doi:10.1016/j.ymssp.2017.01.039.

[27] A. Nateghi, L. Van Belle, C. Claeys, E. Deckers, B. Pluymers, W. Desmet, Wave propagation in locally resonant cylindrically curved metamaterial panels, International Journal of Mechanical Sciences 127 (2017) 73–90. doi:10.1016/j.ijmecsci.2016.07.003.

[28] A. Nateghi, L. Sangiuliano, C. Claeys, E. Deckers, B. Pluymers, W. Desmet, Design and experimental validation of a metamaterial solution for improved noise and vibration behavior of pipes, Journal of Sound and Vibration 455 (2019) 96–117. doi:10.1016/j.jsv.2019.05.009.

[29] C. Droz, O. Robin, M. Ichchou, N. Atalla, Improving sound transmission loss at ring frequency of a curved panel using tunable 3D-printed small-scale resonators, Journal of Acoustical Society of America 145(1) (2019) 72–78. doi:10.1121/1.5088036.

[30] J. Berthaut, Contribution à l'identification large bande des structures anisotropes: application aux tables d'harmonie des pianos, PhD Thesis, 2004, École Centrale de Lyon, France.

[31] G. Inquiété, Numerical simulation of wave propagation in laminated composite plates, PhD Thesis, 2008, École Centrale de Lyon, France.

[32] C. Droz, R. F. Boukadia, M. Ichchou, W. Desmet, Diffusion-based design of locally resonant sub-systems using a reduced wave finite element framework, Proceeding of ISMA 2018 (2018) 2983–2995.

[33] J. H. Rindel, Dispersion and absorption of structure-born sound in acoustically thick plates, Applied Acoustics 41 (1994) 97–111. doi:10.1016/0003-682X(94)90063-9.

[34] S. Thwaites, N. H. Clark, Non-destructive testing of honeycomb sandwich structures using elastic waves, Journal of Sound and Vibration 187 (1995) 253–269. doi:10.1006/jsvi.1995.0519.

[35] L. Brillouin, Wave Propagation in Periodic Structures: Electric Filters and Crystal Lattices, Dover Publications, 1953.

[36] B. R. Mace, D. Duhamel, M. J. Brennan, L. Hinke, Finite element prediction of wave motion in structural waveguides, Journal of the Acoustical Society of America 117 (2005) 2835–2843. doi:10.1121/1.1887126.

[37] E. Manconi, B. R. Mace, Modelling wave propagation in two dimensional structures using finite element analysis, Journal of Sound and Vibration 318 (2008) 884–902. doi:10.1016/j.jsv.2008.04.039.

[38] F. Errico, M. Ichchou, S. D. Rosa, O. Bareille, F. Franco, The modelling of the flow-induced vibrations of periodic flat and axial-symmetric structures with a wave-based method, Journal of Sound and Vibration 424 (2018) 32–47. doi:10.1016/j.jsv.2018.03.012.